Historical and Future Asymmetry of ENSO Teleconnections with Extremes

Ruby Lieber[1,2], Josephine Brown[1,2], Andrew King[1,2], Mandy Freund[3]

[1]*School of Geography Earth and Atmospheric Sciences, University of Melbourne, Parkville, VIC, Australia*

[2]*Australian Research Council Centre of Excellence for Climate Extremes*

[3]*CSIRO Environment, Melbourne, VIC, Australia*

Corresponding author: Ruby Lieber, rlieber@student.unimelb.edu.au

Early Online Release: This preliminary version has been accepted for publication in *Journal of Climate*, may be fully cited, and has been assigned DOI 10.1175/JCLI-D-23-0619.1. The final typeset copyedited article will replace the EOR at the above DOI when it is published.

ABSTRACT

El Niño-Southern Oscillation (ENSO) is the dominant source of climate variability globally. Many of the most devastating impacts of ENSO are felt through extremes. Here we present and describe a spatially complete global synthesis of extreme temperature and precipitation relationships with ENSO. We also investigate how these relationships evolve under a future warming scenario under high greenhouse gas emissions using fourteen models from the Coupled Model Intercomparison Project Phase 6 (CMIP6) ensemble. Firstly, we demonstrate that models broadly capture observed ENSO teleconnections to means and extremes using the Twentieth Century Reanalysis version 3 (20CRv3). The models project that more regions will experience an amplification of the historical ENSO teleconnection with mean temperature and precipitation than a dampening under a high-emissions climate projection. The response of the ENSO teleconnection with extremes is very similar to the mean response, with even larger changes in some regions. Hence, regions that are predicted to experience an amplification of the ENSO teleconnection under future warming can also expect a comparable amplification in the intensity of extremes. Furthermore, models that suggest greater amplification of ENSO amplitude also tend to exhibit greater intensification of teleconnections. Future changes in regional climate variability may be better constrained if changes in ENSO itself are better understood.

1. Introduction

The El Niño-Southern Oscillation (ENSO) is a naturally occurring atmosphere-ocean mode of variability that influences climate and weather globally. ENSO is the dominant source of inter-annual climate variability through its atmospheric teleconnections (McPhaden et al., 2006). ENSO has been shown to impact ecosystems, agriculture, and economies (Anderson et al., 2019; Callahan & Mankin, 2023). Some of the most devasting impacts of ENSO are felt through climate extremes (Goddard & Gershunov, 2020), which remain uncertain particularly in less developed regions (Lieber et al 2022). Many studies have analysed ENSO teleconnections with mean temperature and precipitation patterns (Bonfils et al., 2015; McGregor et al., 2022; Perry et al., 2017; Power et al., 2013; Ropelewski & Halpert, 1987), however, there have been few teleconnection studies examining the influence on extremes.

Accepted for publication in *Journal of Climate.* DOI 10.1175/JCLI-D-23-0619.1.

Via remote teleconnections, ENSO influences temperature and precipitation patterns around the world (Ropelewski & Halpert, 1987), most prominently in parts of Australia, North America, South America, and Africa. El Niño, the warm phase of ENSO, is usually associated with above-average global-average temperature and can greatly influence global drought conditions (Vicente-Serrano et al., 2011), with the likely spatial extent of tropical drought more than doubling during a strong El Niño (Lyon, 2004). Meanwhile La Niña, the cool phase of ENSO, can lead to intensified annual floods in around a third of the global land area (Ward et al., 2014). Some regions do experience the opposite effects, for example California is more prone to increased precipitation leading to flooding during El Niño (Cayan et al., 1999) and reduced rainfall and increased risk of drought during La Niña (Allen & Anderson, 2018). The impacts of El Niño and La Niña are often opposite in sign, however the impacts are not necessarily the inverse of each other (Frauen et al., 2014). Southeast Australia, for example, receives less rainfall during El Niño and more rainfall during La Niña than on average conditions. Nevertheless, the intensity of an El Niño event is not correlated with the magnitude of drying whereas the intensity of the rainfall associated with a La Niña is closely linked to the strength of the event in this region (Chung et al., 2023; Chung & Power, 2017; Freund et al., 2021; Power et al., 2006).

In a future warmer climate, ENSO teleconnections are projected to move eastward in coupled global climate model simulations with enhanced precipitation in the central and eastern Pacific Ocean and enhanced drying in the western Pacific Ocean (Bonfils et al., 2015; Chen et al., 2023; Power et al., 2013; Stevenson, 2012). The spatial extent of ENSO teleconnections with mean temperature and precipitation in Coupled Model Intercomparison Project Phase 5 (CMIP5) models (Taylor et al., 2012) has been shown to increase over the global land area under a high-emissions scenario (Perry et al., 2017), however changes to the strength of the teleconnection are unclear (Perry et al., 2020). It has been suggested that ENSO teleconnections will intensify in the future when examining teleconnections with Coupled Model Intercomparison Project Phase 6 (CMIP6) (Eyring et al., 2016) models under continued global warming. McGregor et al. (2022) found that ~50% of the global land areas with significant teleconnections will experience a change in the strength of the mean temperature and precipitation teleconnection (defined using linear regressions with Niño3.4 index), with most of the impacted regions experiencing an amplification rather than a dampening. Regional teleconnections have also been shown to intensify in many land regions

Accepted for publication in *Journal of Climate.* DOI 10.1175/JCLI-D-23-0619.1

independent of changes in SST variability in a climate model large ensemble (Fasullo et al., 2018),

Extreme weather events are defined as statistically rare events and are important to understand as they can have large impacts (Seneviratne et al., 2021). Observed trends in historical extreme daily temperature show increases in both maximum and minimum temperature since the mid-20th century (Alexander et al., 2006; Donat et al., 2016; Dunn et al., 2020). The magnitude of the trend in minimum temperature is larger than the trend in maximum temperature and is present over a larger land area. It has also been suggested that extreme 1-day precipitation has intensified, however the changes are less spatially coherent than the temperature trends (Alexander et al., 2006; Donat et al., 2016; Dunn et al., 2020; Westra et al., 2013). Positive trends in global temperature and precipitation extremes over the historical period have also been found in reanalysis and model simulations (Donat et al., 2016; Sillmann et al., 2013). Temperature extremes are projected to increase over the global land area in CMIP5 and CMIP6 models under all future warming scenarios (Ajjur & Al-Ghamdi, 2021; Li et al., 2021; Sillmann et al., 2013). Like the difference in magnitude of the trend found in the historical period, projected changes to cold extremes are found to be larger than those to hot extremes. CMIP5 and CMIP6 models also project an increase in the intensity of monthly and annual rainfall extremes globally (Feng et al., 2023; Li et al., 2021; Sillmann et al., 2013).

It is important to consider changes in ENSO and associated teleconnections when investigating changes in past and future extremes as ENSO has been shown to have influence on both temperature and precipitation extremes (Kenyon & Hegerl, 2008, 2010). ENSO impacts cold and hot extremes differently. Many regions such as Australia, southern Asia, Canada, and South Africa experience significantly cooler maximum temperatures during La Niña while parts of the United States and southern South America experience significantly warmer maximum temperatures during this ENSO phase (Arblaster & Alexander, 2012). Less work has been done documenting ENSO's global influence on minimum temperature extremes, although studies have found correlations between ENSO phase and the spatial and temporal occurrence of frost (Crimp et al., 2015; Müller et al., 2000). ENSO is the dominant climate phenomenon influencing precipitation extremes globally and has been shown to impact extreme rainfall in parts of North and South America, southern and eastern Asia, South Africa, Australia, and Europe (Gershunov & Barnett, 1998; Huang & Stevenson, 2023;

Accepted for publication in *Journal of Climate.* DOI 10.1175/JCLI-D-23-0619.1

Min et al., 2013; Sun et al., 2015; Yeh et al., 2018). Like with ENSO's teleconnection with mean precipitation, the impact of ENSO on extreme precipitation is not symmetrical between El Niño and La Niña, and some regions e.g., southeast China, southeast South America, and South Africa, only have a significant effect for a single active phase (Sun et al., 2015).

Many global studies on ENSO teleconnections with mean and extreme climate use continuous ENSO indicators expressed by indices such as the Niño3.4 index or a Principal Component, including changes in both phases of ENSO in a single measure of the anomaly, when investigating future changes (Fasullo et al., 2018; Hao et al., 2018; McGregor et al., 2022; Perry et al., 2017). Continuous teleconnection studies through correlation or regression do not consider the differences between El Niño and La Niña teleconnections. It is not clear from these analyses if the amplification of El Niño and La Niña precipitation and temperature anomalies will be equivalent or if changes will be greater in one phase than another due to event amplitude asymmetry (Burgers & Stephenson, 1999). There is also limited comparison between evolution of ENSO teleconnections with mean climate and teleconnections with extremes on a global scale.

Regional studies on ENSO teleconnections with extremes have investigated similarities with the mean teleconnection and historical changes, however, there are limited studies looking at projections. In South America, ENSO has been linked to extreme rainfall and drought over Brazil (Costa et al., 2021; Grimm et al., 2020; Jimenez-Munoz et al., 2016) and extreme rainfall and temperature in Argentina (Grimm & Tedeschi, 2009; Rusticucci et al., 2017). ENSO-driven extreme events are expected to increase in frequency in regions with a robust ENSO signal in the current climate (Cai et al., 2020). In North America, developing La Niña's are associated with more summer heat extremes (Luo & Lau, 2020) and drought in the southeast (Mo & Schemm, 2008). Extreme precipitation patterns have a strong response to ENSO phase, with more extreme rainfall in the Southwest (Northwest) during El Niño (La Niña), similar to that of the mean precipitation pattern (Cayan et al., 1999; Zhang et al., 2010). The frequency and intensity of ENSO-driven extreme precipitation and both drought and flood events are expected to increase over California under global warming (Huang & Stevenson, 2023; Yoon et al., 2015). In Australia, the ENSO influence on seasonal extremes of rainfall and temperature resembles the influence on mean climate (Min et al., 2013). In tropical regions, El Niño events have been associated with severe drought and extreme maximum temperatures (Rifai et al., 2019), with greater impacts on maximum temperatures

Accepted for publication in *Journal of Climate.* DOI 10.1175/JCLI-D-23-0619.1

than minimum temperatures found in Malaysia (Tan et al., 2021). ENSO has a pronounced seasonal influence on extreme precipitation that is generally consistent with its influence on seasonal mean precipitation in Malaysia, Indonesia, and the Philippines (Supari et al., 2018; Tangang et al., 2017; Villafuerte et al., 2015). ENSO has been found to be the dominant driver of seasonal mean and extreme precipitation variability in the Yangtze River basin (Xiao et al., 2015; Zhang et al., 2014) and El Niño leads to increased frequency and duration of heatwaves over China (Luo & Lau, 2019). The ENSO influence on extremes over Africa has been shown to be stronger for temperature than precipitation with a strong correlation between ENSO and DJF maximum temperature extremes found in northeast Africa and a slightly weaker correlation for minimum temperature extremes (Donat et al., 2014). This relationship was also found in South Africa as well as a strong link between ENSO and drought (Meque & Abiodun, 2015).

Here we investigate how the ENSO teleconnection with mean climate will evolve in the future and if the same evolution applies to extremes. First, we discuss global ENSO teleconnections with the mean and extremes using a reanalysis product. Then, we evaluate the ability of 14 CMIP6 models to simulate historical ENSO teleconnections with the mean and extremes in comparison with the reanalysis. Finally, we use these models to look at projections of ENSO teleconnections with the mean and extremes. The following questions are addressed: Do CMIP6 models simulate the observed ENSO teleconnections with extremes? Do changes in ENSO teleconnections with extremes scale with changes in ENSO teleconnections with mean temperature and precipitation? Are changes in El Niño and La Niña teleconnections with extremes of the same magnitude or are changes larger for one phase?

2. Data and Methods

a. Datasets

1) HadEX3

We use the HadEX3 dataset as our observational reference for extremes (Dunn et al., 2020). HadEX3 is a global station-based gridded dataset of land-based extremes. It is comprised of monthly temperature and precipitation extremes from 1901-2018 on a 1.25° x 1.875° grid and is suitable for comparison with reanalysis and global climate model output (Donat et al., 2016; Dunn et al., 2022).

Accepted for publication in *Journal of Climate.* DOI 10.1175/JCLI-D-23-0619.1

2) TWENTIETH CENTURY REANALYSIS

The National Oceanic and Atmospheric Administration, Cooperative Institute for Research in Environmental Sciences and the U.S Department of Energy Twentieth Century Reanalysis version 3 (NOAA-CIRES-DOE 20CRv3) is used to assess the historical teleconnection between ENSO and temperature and precipitation variables as in-situ observational datasets, such as HadEX3, are not spatially and temporally complete (Slivinski et al., 2019). 20CRv3 has a large 80-member ensemble and covers the period 1836 to 2015 with spatial resolution of 0.7° latitude and longitude. The Twentieth Century Reanalysis uses prescribed SSTs from the Met Office Hadley Centre Global Sea Ice and SST (HadISST) reanalysis (Rayner et al., 2003) and assimilates surface pressure using an Ensemble Kalman Filter method. As ENSO events occur on a 2–7-year cycle a long time series is needed to ensure an adequate sample size of El Niño and La Niña events for robust analysis. Hence, we use the full century in our analysis despite the known lack of observations before 1950 in both 20CRv3 and HadISST (Rayner et al., 2003; Slivinski et al., 2019). The sub-daily reanalysis output allows for calculation of the extreme indices. Here we use monthly temperature and precipitation from 20CRv3 (Slivinski et al., 2019) from 1900-2014 and three extreme indices (Maximum value of daily maximum temperature (TXx), Minimum value of minimum daily temperature (TNn), Maximum 1-day precipitation (Rx1day)) calculated from 3-hourly temperature and precipitation data also from 20CRv3 from 1900-2014. The reanalysis data was conservatively remapped from a 1° x 1° latitude-longitude grid to a 1.5° x 1.5° grid to allow for comparison with model data from CMIP6 on the same grid.

The ability of 20CR to simulate regional temperature and precipitation variability has previously been evaluated against observations, satellite data, and other reanalysis products. It has been shown to reliably produce interannual variability of air temperature and precipitation fields on climate timescales (Slivinski et al., 2021). We also compare 20CR with HadEX3 to assess skill in capturing ENSO-extreme teleconnection patterns (Dunn et al., 2020). We find that 20CR performs better at capturing the spatial pattern of temperature extremes than precipitation extremes and does better at capturing the El Niño pattern than the La Niña pattern (Figure S1, S2). Overall, pattern correlation values are generally moderate-high (>0.5 for all composites). Hence 20CR is appropriate to use as a baseline for historical climate when assessing CMIP6 models for this study. A known bias within the reanalysis is a

Accepted for publication in *Journal of Climate.* DOI 10.1175/JCLI-D-23-0619.1

persistent tropical precipitation bias that overestimates precipitation rates and leads to the appearance of a double Intertropical Convergence Zone (ITCZ) (Slivinski et al., 2019). Over land, correlations between 20CR and observational products are high, and interannual variability is captured well, although 20CR tends to overestimate precipitation in most of North America and underestimate it over Australia (Slivinski et al., 2021). The uncertainty in ENSO teleconnections in 20CR is also larger over regions of limited data, including much of the Global South (Lieber et al. 2022). As each ensemble member realisation represents a different possible weather scenario, we take the ensemble average when using composites to reduce the noise from random weather fluctuations to make it easier to identify underlying climate patterns.

3) CMIP6

Fourteen models from CMIP6 were used in this study (See Table S1 for list of models). This subset of models was chosen because they each have data for the historical experiment (1900-2014) and future scenario SSP5-8.5 (2015-2100) for all the variables required, namely mean surface temperature (ts), mean precipitation (pr), TXx, TNn, and Rx1day. SSP5-8.5 refers to the Shared Socioeconomic Pathway (SSP) with the highest emissions that results in a radiative forcing of approximately 8.5 Wm^{-2} in the year 2100 (O'Neill et al., 2016). While this scenario has been deemed implausible (Hausfather & Peters, 2020), we use it as we would expect it to have the clearest human-induced climate change signal, and for ease of comparability with other studies which often use this scenario. One ensemble member, r1i1p1f1, was used for each model (the influence of including different ensemble members was tested on results and is further explained in section 3.c.). The variables ts and pr were re-gridded onto a consistent 1.5° x 1.5° grid prior to evaluation. The three extreme indices used were previously calculated by the Centre for International Climate and Environmental Research (CICERO) for all models that had the available daily resolved data required to calculate the indices (Sandstad et al., 2022). These extreme indices were calculated on the model's native grid and then remapped onto a 1.5° x 1.5° grid using a conservative method consistent with (Kim et al., 2020). The order of calculating and regridding extremes has been shown to influence results, however, this is mostly observed in return period estimates and has little impact on long term trends and variability (Avila et al., 2015).

Accepted for publication in *Journal of Climate*. DOI 10.1175/JCLI-D-23-0619.1

The CMIP6 ensemble has been shown to adequately simulate ENSO dynamics and ENSO teleconnections with the mean climate, although with varying skill between models (Freund et al., 2020; Grose et al., 2020; Planton et al., 2021). CMIP6 models generally outperform CMIP5 models on a range of metrics characterising ENSO, including the teleconnection metrics (Planton et al., 2021). However, improvement in capturing teleconnections does not necessarily mean improvement in simulating the underlying dynamics that govern them (Planton et al., 2021). Persistent model biases in CMIP6 include the "cold-tongue bias" in which the cool equatorial Pacific Ocean waters extend too far westwards (Jiang et al., 2021). Consequently, modelled easterly trade winds are also shifted westward and are too strong in the western Pacific and too weak in the central Pacific. This is associated with a dry bias in modelled precipitation over the western Pacific (Planton et al., 2021). The CMIP6 ensemble has been evaluated in its ability to simulate a range of extreme indices against HadEX3, reanalysis products, and CMIP5 (Kim et al., 2020). No significant improvements were found in CMIP6 over CMIP5 when comparing global extreme climatology patterns and the models generally capture the observed extreme patterns at the global and regional scale. Biases in temperature extremes persist such as a cold bias in cold extremes over high latitudes, and a dry bias in extreme rainfall over the tropics (Kim et al., 2020).

b. Methods

All temperature datasets are detrended using a quadratic detrending method to remove the warming trend that is observed since 1950. Prior to removing the trend, each model's future SSP5-8.5 run was stitched together with its historical run and the trend calculated over the entire time series (1900-2100). This allows us to better capture the long-term trends in the data and maintain temporal continuity.

1) ETCCDI INDICES

Three indices from the suite defined by the Expert Team on Climate Change Detection and Indices (ETCCDI) in Zhang et al. (2011) are used in this study to characterize extremes. We consider the "maximum value of daily maximum temperature" (TXx) as a measure of the temperatures found on the hottest day of the month. The "minimum value of daily minimum" (TNn) describes the coldest night of the month. The "maximum 1-day precipitation" (Rx1day) is used to represent extreme precipitation. Rx1day is chosen over

Accepted for publication in *Journal of Climate.* DOI 10.1175/JCLI-D-23-0619.1

other multi-day extreme precipitation indices such as Rx5day (maximum 5-day precipitation) as Rx1day tends to respond more rapidly to climate forcings (Kirchmeier-Young & Zhang, 2020; Min et al., 2011). We choose these three indices as they may be defined monthly on a spatial grid, and they are widely used and easy-to-understand metrics for extremes. This allows for correlation and composite analysis with other monthly indices like the Niño3.4 index commonly used to describe ENSO.

2) ENSO INDEX

The Niño3.4 index is calculated for each model from SST anomalies in the Niño3.4 region defined as the area between 5°S-5°N and 170-120°W (Trenberth, 1997). Monthly anomalies were calculated using a climatology of 1950-1979. ENSO event years are then found for each model using their normalised Niño3.4 index. Events are defined when the index is sustained above 0.5 (or below -0.5) standard deviations for at least six months. The HadISSTv1 data set is used when calculating the Niño3.4 index for 20CR as 20CR uses prescribed SSTs from the HadISST data set (Compo et al., 2011; Slivinski et al., 2019).

3) COMPOSITES

El Niño and La Niña composites are produced for each model and for the reanalysis. Composite analysis allows for the consideration of the asymmetry in the teleconnection between each phase. We consider El Niño (or La Niña) anomalies relative to all years. The El Niño composite is produced by calculating the December to February (DJF) seasonal average in all El Niño years and subtracting the DJF seasonal average in all years. The same is done for La Niña. The 20CR composites are constructed from the ensemble average following the same method as the models.

4) CORRELATIONS

Spatial correlations are used to define the strength of the ENSO teleconnection to exclude regions with non-significant correlation. The correlation between the Niño3.4 index and each temperature and precipitation variable are calculated for each grid point using a Pearson's correlation. The correlation is calculated from the DJF seasonal average Niño3.4 index and DJF seasonal average anomalies. We focus on DJF as this is the season when ENSO events usually peak. Grid points where the absolute value of Pearson's correlation coefficient is less than 0.2 are masked and not considered in parts of this study.

Accepted for publication in *Journal of Climate.* DOI 10.1175/JCLI-D-23-0619.1

3. Results and Discussion

a. Historical ENSO teleconnection with temperature and precipitation extremes in reanalysis and CMIP6

ENSO teleconnections with extremes are explored in the 20CR ensemble mean to provide a baseline for comparison with CMIP6 models. The teleconnections are evaluated using composites of El Niño and La Niña states, defined as described in Section 2.b.3.

1) OBSERVED ENSO TELECONNECTIONS WITH EXTREMES IN 20CR

Both El Niño and La Niña phases of ENSO display a teleconnection with DJF extreme temperature (TXx, TNn) and precipitation (Rx1day) indices globally in the historical period (Figure 1, Figure 2). The hottest days (TXx) are generally anomalously hot during El Niño in regions where average daily temperatures are also anomalously hot such as Australia, South Africa, and northern South America (Figure 1a, c). These regions also experience the opposite during La Niña (cooler average daytime temperatures and cooler maximum temperatures, Figure 1b, d). There are some exceptions however, in northern North America mean temperatures are anomalously hot during El Niño, but TXx is not. When assessing the magnitude of the relative temperature anomalies, the relationship between ENSO and the coldest days (TNn) is not as strong over land in many regions where ENSO is known to have a strong influence (e.g., South Africa, Australia, northern South America), however is very strong over North America (Figure 1e, f). El Niño and La Niña are seen to influence extreme one day rainfall (Rx1day) in much the same way as average rainfall with regions such as Australia, South Africa, and Northern South America experiencing below average maximum one day rainfall totals in El Niño (Figure 2a, c) and above average in La Niña (Figure 2b, d).

Comparing the teleconnections in 20CR with the HadEX3 composites, there are several regions where the sign of the anomaly is opposite across datasets (Figures S1, S2). For the El Niño TXx and TNn composite in HadEX3, there is a negative temperature anomaly in northeastern Africa, above the horn, however in 20CR there is a positive temperature anomaly. For TNn there is a positive anomaly in southeastern South America but a negative one in 20CR. There are also several patches over Europe where the sign disagrees, however this region is not as highly correlated with ENSO and so teleconnections are weaker.

Accepted for publication in *Journal of Climate.* DOI 10.1175/JCLI-D-23-0619.1

For La Niña there are also patches of disagreement on the sign of the anomaly for TXx and TNn in northeastern Africa, Australia, South and North America, however they are less spatially coherent than for El Niño. For the Rx1day composites, there are patches of disagreement across all continents for El Niño and La Niña. The largest region of disagreement is in West Africa, where HadEX3 has a negative rainfall anomaly in El Niño and 20CR has a positive rainfall anomaly. The opposite is also found for La Niña.

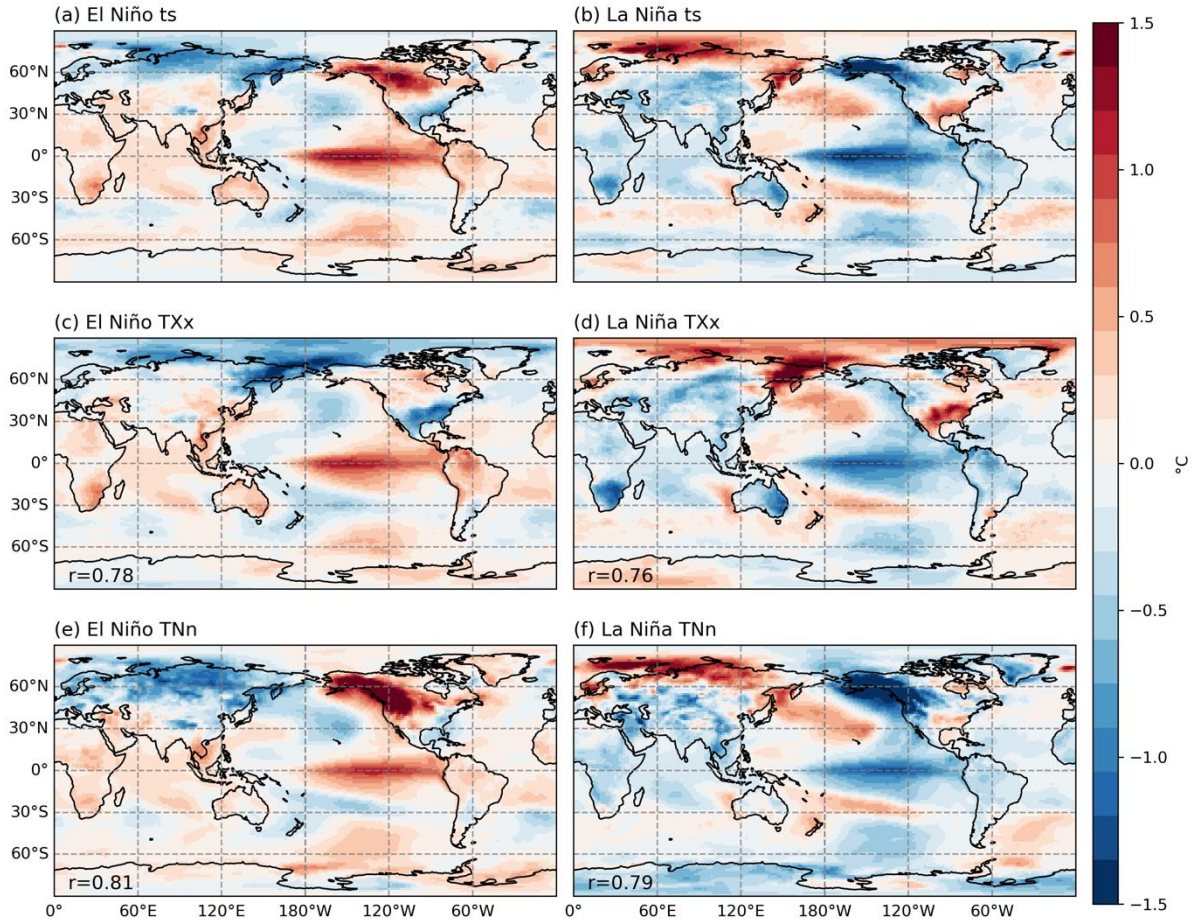

Figure 1: 20CR ensemble mean composites of DJF seasonal mean and extreme temperatures during El Niño and La Niña events for the period 1900-2014 in °C. Panels depict a) El Niño ts, b) La Niña ts, c) El Niño TXx, d) La Niña TXx, e) El Niño TNn and f) La Niña TNn. R values in bottom left of extreme composite represent pattern correlation with mean composite.

Accepted for publication in *Journal of Climate.* DOI 10.1175/JCLI-D-23-0619.1

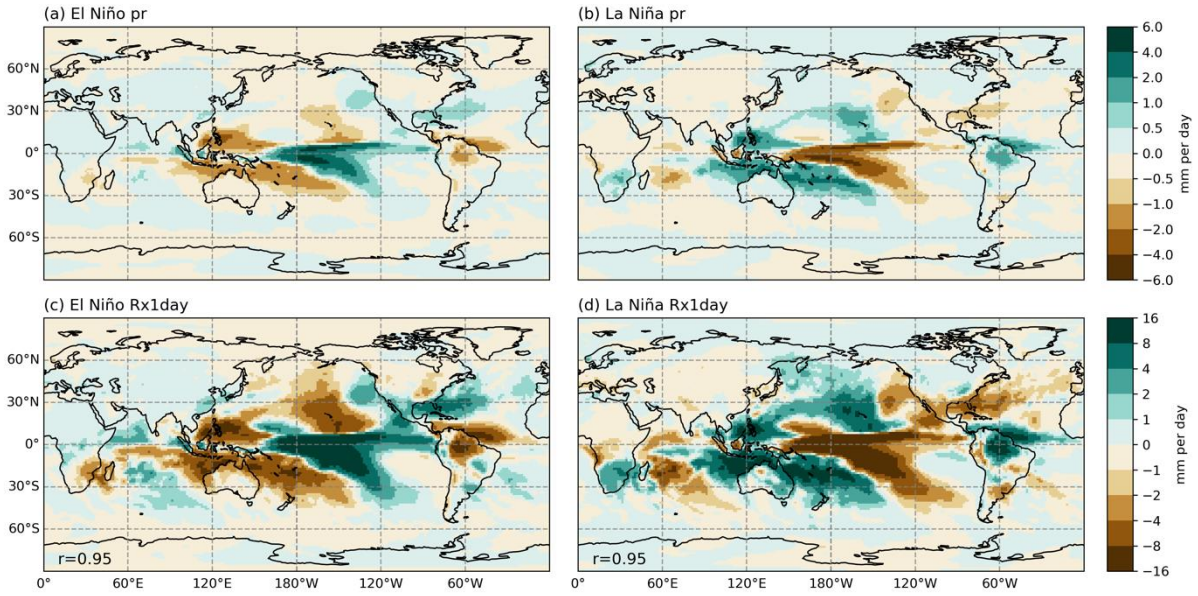

Figure 2: 20CR ensemble mean composites of DJF seasonal mean and extreme precipitation during El Niño and La Niña events for the period 1900-2014 in mm/day. Panels depict a) El Niño pr, b) La Niña pr, c) El Niño Rx1day and d) La Niña Rx1day. R value in bottom left of extreme composite represent pattern correlation with mean composite.

2) ENSO TELECONNECTIONS WITH EXTREMES IN CMIP6 HISTORICAL RUNS

The teleconnection between ENSO and DJF extreme temperature and precipitation in CMIP6 models is also calculated (Figure 3, Figure 4). The CMIP6 models demonstrate varying skill at capturing the anomaly patterns in the temperature composites in comparison with 20CR as measured using the pattern correlation coefficient between models and 20CR over the global domain (Supplementary Table S1). For El Niño, the CMIP6 multi model mean (MMM) captures the location and magnitudes of SST anomalies in agreement with 20CR, although they extend slightly further westwards than in the reanalysis (Figure 3a), consistent with the cold tongue bias commonly found in CMIP models (Bellenger et al., 2014; Li & Xie, 2014). The MMM largely captures the correct location and sign of the mean temperature anomalies but overestimates the magnitude in South Africa, Australia, India, northern South America, and North America. In South Africa, the location of the teleconnection is shifted too far westward and in northern South America it is too far eastward (Figure S3). For La Niña, the MMM overestimates the magnitude of the mean temperature anomalies in Australia and northern South America and underestimates them in South Africa and northwestern North America (Figure 3b). The location of the La Niña teleconnection is shifted to the west over Australia. The same biases are found in the TXx teleconnection (Figure 3c, d). For the TNn teleconnection, the MMM underestimates the

Accepted for publication in *Journal of Climate*. DOI 10.1175/JCLI-D-23-0619.1

magnitude of the anomalies in North America during El Niño and La Niña (Figure 3e, f). Using pattern correlation as a measure of performance, some models do a better job of capturing the El Niño pattern while others do a better job of the La Niña pattern (Supplementary Table S1). For example, ACCESS-CM2, GFDL-CM4, GFDL-ESM4, MRI-ESM2-0, NorESM2-LM, and NorESM2MM are consistently better at capturing El Niño patterns, which we would expect as El Niño teleconnections are generally stronger than La Niña (Chen et al., 2017; Frauen et al., 2014), however, BCC-CSM2-MR, CanESM5, MIROC6, and MPI-ESM1-2-HR are consistently better at capturing La Niña patterns across all temperature variables, which may be because models struggle with capturing event amplitude asymmetry and persistence of events (Planton et al., 2021).

Most models capture the 20CR mean precipitation and Rx1day composite patterns well based on global pattern correlations above 0.5 (Supplementary Table S2). However, the CMIP6 MMM (Figure 4a) underestimates the magnitude of the precipitation anomalies in the western Pacific, some parts of the Maritime Continent (consistent with Chen et al. (2023)), Venezuela and eastern South Africa during El Niño (Figure S4). This is characteristic of the 'dry equator bias' commonly found in CMIP models and is linked to the cold tongue bias which alters the location of convective precipitation along the equator (Planton et al., 2021). The MMM overestimates the rainfall anomalies over northern South America, the western part of the Maritime Continent and over Australia. This is also true for La Niña (Figure 4b). The MMM over and underestimates the Rx1day anomalies in the same regions as the precipitation anomalies for both phases (Figure 4c, d).

When comparing the CMIP6 MMM with HadEX3, the TXx composites are moderately correlated, however the TNn and Rx1day composites are strongly correlated (Figure S1, S2). The MMM extreme temperature composites are generally more highly correlated with the HadEX3 composites than the 20CR composites, but the extreme rainfall composites are more highly correlated with 20CR (Table S1, S2, Figure S1, S2). There are regions where the sign of the HAdEX3 anomaly and CMIP6 MMM anomaly are of opposite sign, most notably in northeastern Africa (where HadEX3 was also in disagreement with 20CR), as well as several other regions where 20CR and HadEX3 agreed. Therefore, the model's ability to accurately simulate ENSO teleconnections with extremes is in part dependent on the reference dataset used, and observational uncertainty is likely a factor in discrepancies between observed and modelled teleconnections.

Accepted for publication in *Journal of Climate.* DOI 10.1175/JCLI-D-23-0619.1

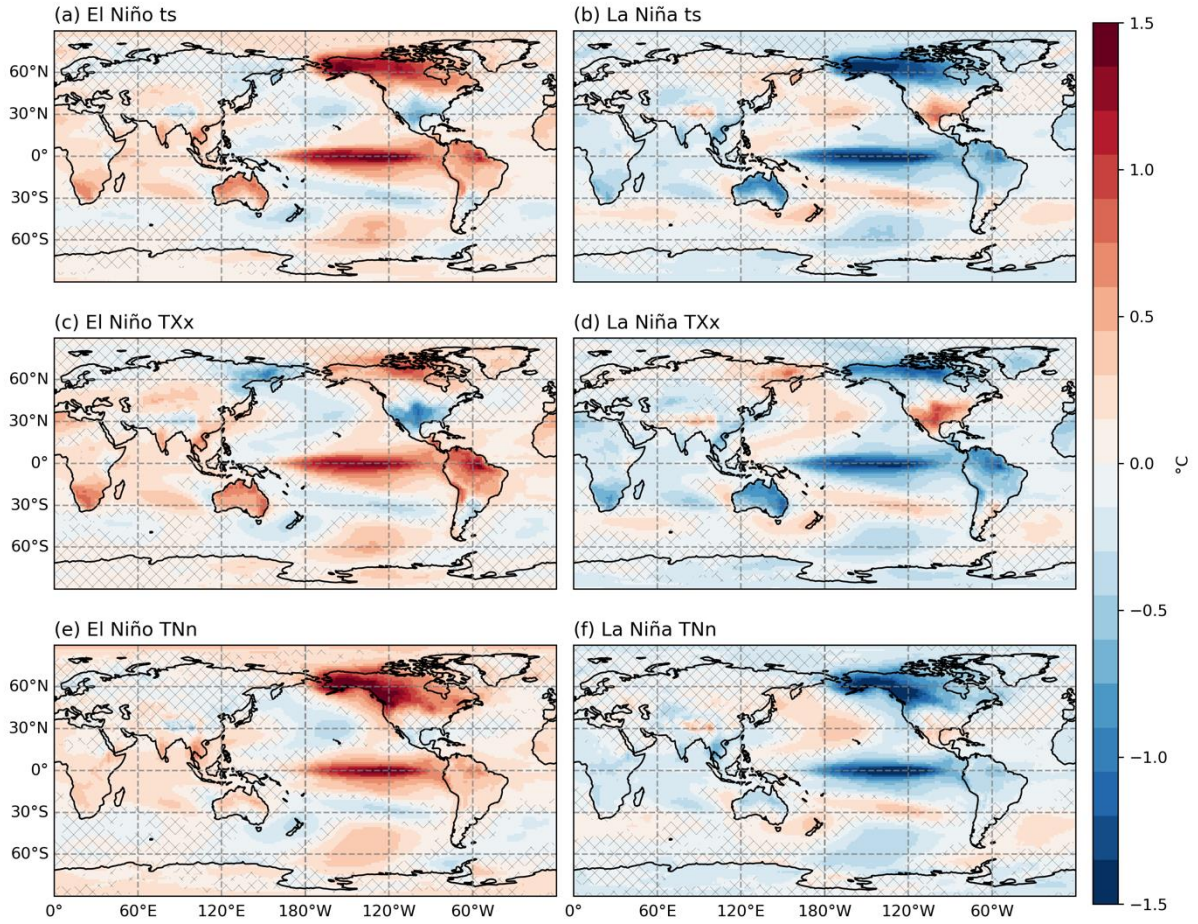

Figure 3: Same as for Figure 1 but for the CMIP6 multi model mean. Hatching indicates low model agreement based on a 75% threshold.

Accepted for publication in *Journal of Climate.* DOI 10.1175/JCLI-D-23-0619.1

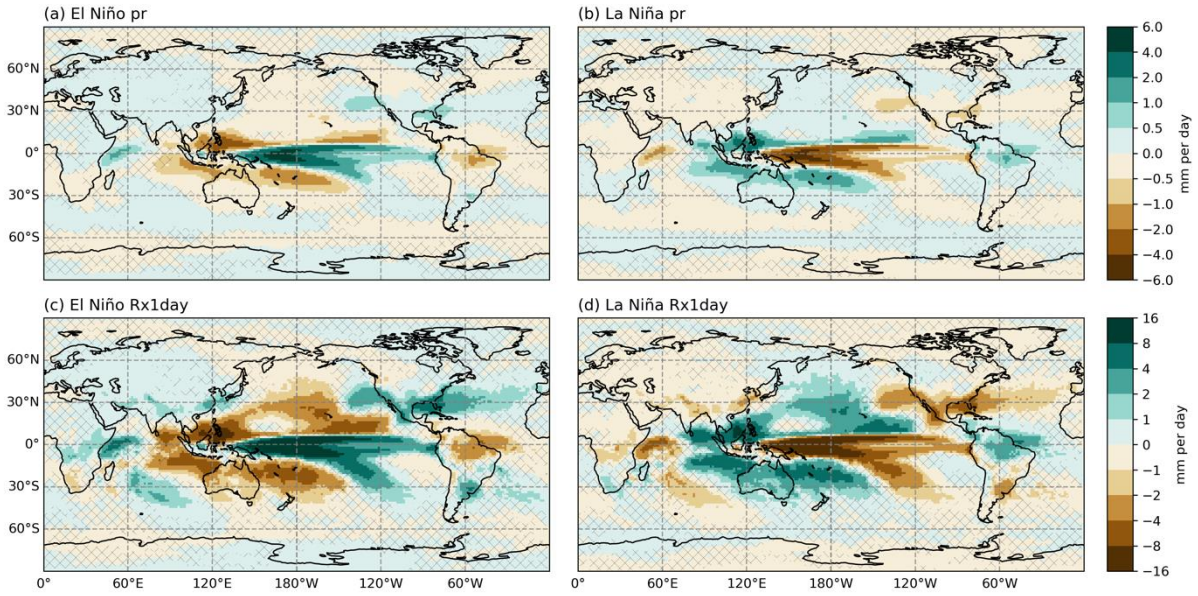

Figure 4: Same as for Figure 2 but for the CMIP6 multi model mean. Hatching indicates low model agreement based on a 75% threshold.

3) COMPARING DJF MEAN AND EXTREME TELECONNECTIONS IN 20CR AND CMIP6

The sign of the mean and extreme teleconnection pattern is compared at the regional scale for both reanalysis and models to determine how closely these patterns are related in more detail. For the 20CR reanalysis, the TXx anomaly pattern is very similar to the mean temperature anomaly pattern in both El Niño and La Niña (Figure 5a, b). The TNn pattern is also similar to the mean pattern however there are some regional differences (Figure 5c, d). Comparing the sign between the ts El Niño composite and the TNn composite at the grid point level in 20CR reveals that the sign of the teleconnection with TNn is opposite to that of the mean in south-eastern Australia and central America. In the case of south-eastern Australia, this implies that mean temperatures are usually warmer during El Niño, but minimum temperatures are usually colder. The opposite is found for La Niña, mean temperatures are cooler but minimum overnight temperatures are warmer. We also find the same relationship for mean minimum temperature (TN, see Supplementary Figure S5). This could be explained by changes in cloud cover in these regions e.g., in Australia, during La Niña there is increased cloudiness which can act to trap heat, whereas there are more frequently clear skies during El Nino (Jones & Trewin, 2000). These regional differences in the sign of the anomalies are also captured by the CMIP6 multi model mean (see Supplementary Figure S6). The 20CR Rx1day composites are very similar to the mean

Accepted for publication in *Journal of Climate*. DOI 10.1175/JCLI-D-23-0619.1

precipitation composites and there are some regions where the strength of the teleconnection with the extreme is stronger than that of the mean (South Africa, Australia, northern South America and western North America, Figure 6). There are no notable regions where the sign of the teleconnection is different between the mean and extreme case in the 20CR ensemble. The same is found for the CMIP6 MMM (see Supplementary Figure S7).

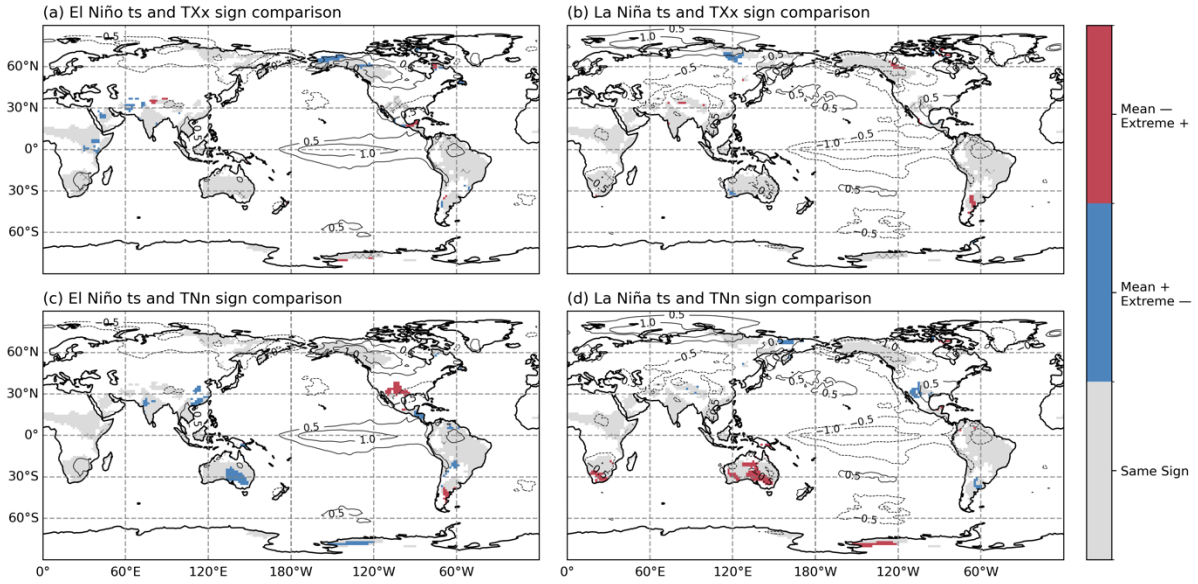

Figure 5: Spatial sign comparison of regional mean and extreme seasonal DJF temperature anomalies during El Niño and La Niña events using 20CR ensemble mean over the period 1900-2014. Panels display the sign agreement between a) El Niño ts and TXx b) La Niña ts and TXx c) El Niño ts and TNn d) La Niña ts and TNn. Grey regions indicate agreement on the sign of the anomaly between the mean and the extreme, while regions with differing signs are color-coded. Red indicates the mean temperature anomaly is negative and the extreme anomaly is positive. Blue indicates the mean temperature anomaly is positive and the extreme anomaly is negative. Contours show the DJF seasonal mean surface temperature anomalies. Hatching indicates regions where the strength of the extreme teleconnection (defined using correlation coefficient) is greater than the mean teleconnection. Regions with correlation < |0.2| are masked.

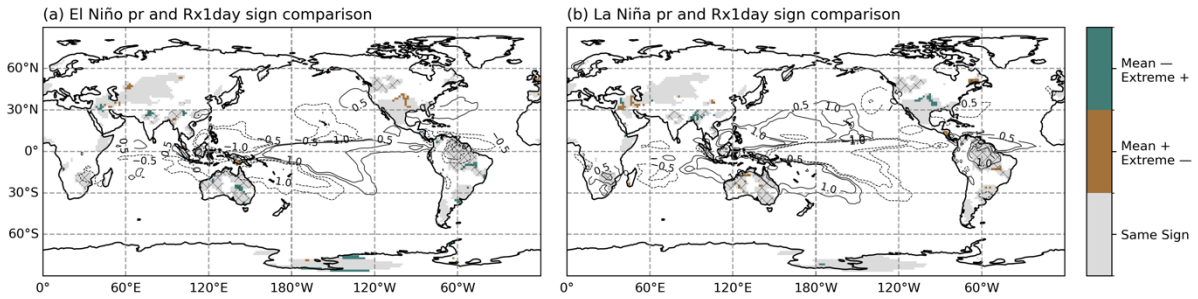

Figure 6: Spatial sign comparison of regional mean and extreme seasonal DJF precipitation anomalies during El Niño and La Niña events using 20CR ensemble mean over the period 1900-2014. Panels display the sign agreement between a) El Niño pr and Rx1day b) La Niña pr and Rx1day. Colors, contours and hatching are the same as for Figure 5 except for precipitation.

Accepted for publication in *Journal of Climate*. DOI 10.1175/JCLI-D-23-0619.1

b. Amplification of ENSO teleconnections under SSP5-8.5 similar in mean and extreme climate

The change in DJF ENSO teleconnections to both mean and extreme climate is evaluated here using CMIP6 simulations under the very high greenhouse gas concentration SSP5-8.5 scenario (Figure 7, Figure 8). We evaluate the change by subtracting the historical composite ENSO teleconnection from the future composite for each of ts, TXx, TNn, pr, and Rx1day. Hatching indicates regions of high model agreement on the sign of the change (based on a threshold of 75%). The largest changes in the MMM teleconnection strength (using magnitude of anomalies as an indicator) for mean and extreme temperatures are over land, consistent with the hypothesis of Fasullo et al. (2018) that the lower heat capacity of the land surface would lead to a greater amplification of terrestrial teleconnections. Over Australia, Africa, Southeast Asia, and northern South America the mean temperature teleconnection intensifies for El Niño (consistent with the findings of Fasullo et al. (2018)). That is, warm anomalies get warmer and cold anomalies get colder. There is a dampening of the teleconnection over north-western North America and Central America. This is consistent with the findings of Beverley et al. (2021) who found this dampening was related to changes to the anomalous circulation over the North Pacific driven by the projected eastward shift of ENSO precipitation. Noticeable differences in the La Niña anomalies, compared to El Niño, includes an amplification rather than a dampening over Central America, and a dampening rather than amplification over eastern Australia and South Africa, however, there is low model agreement in these regions.

In the case of the ENSO teleconnections with extremes, TXx and TNn both amplify and dampen in the same regions as mean temperature, except for TNn over northwest North America which amplifies in La Niña (Figure 7). Contrasting changes between the mean and extreme are also found within one model with multiple ensemble members (Figure S8). Over the ocean, the SST anomalies strengthen in the central Pacific near the Equator, consistent with the projected increasing ENSO amplitude in CMIP6 models (Cai et al., 2022). We find that mean precipitation anomalies amplify over northern Australia, parts of Southeast Asia, western central Asia, east Africa, southeast South America, and northeast South America (Figure 8). We also find a dampening over western South Africa, Central America, and western North America. These amplifications and dampenings are found in both active ENSO phases and are consistent with the findings of McGregor et al. (2022) who proposed amplifications and dampenings were linked to the projected eastward shift and intensification

Accepted for publication in *Journal of Climate.* DOI 10.1175/JCLI-D-23-0619.1

of equatorial precipitation and an associated eastward shift in upper atmosphere velocity potential. We find similar results for Rx1day, suggesting that ENSO-induced extreme rainfall will generally amplify and dampen in the same regions as ENSO teleconnections with mean rainfall.

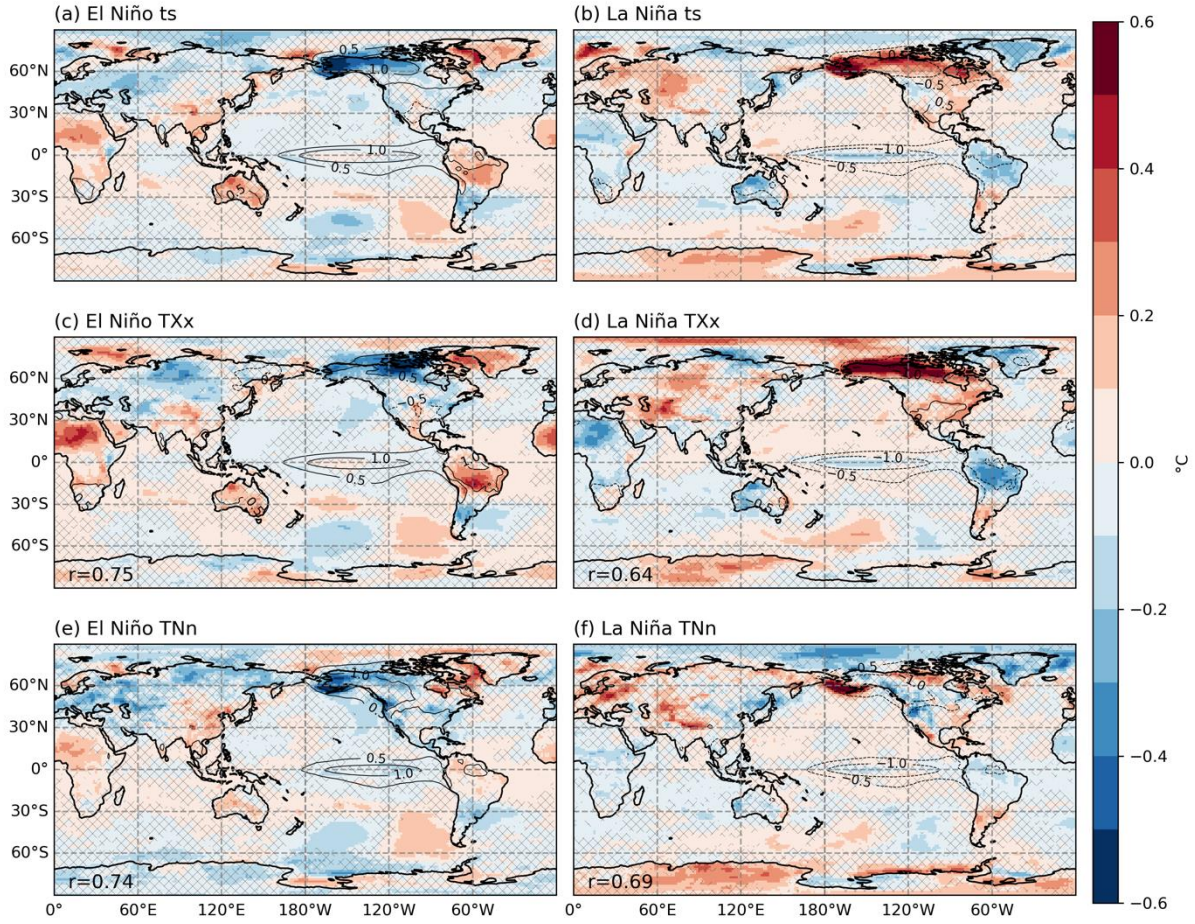

Figure 7: CMIP6 multi model mean composites of change in DJF seasonal mean and extreme temperatures during El Niño and La Niña events under SSP5-8.5 in °C. Change is future composite (2015-2100) relative to the historical composite (1900-2014). Panels depict a) El Niño ts, b) La Niña ts, c) El Niño TXx, d) La Niña TXx, e) El Niño TNn and f) La Niña TNn. R value in bottom left of extreme composite represent pattern correlation with mean composite. Contours depict historical teleconnection.

Accepted for publication in *Journal of Climate.* DOI 10.1175/JCLI-D-23-0619.1

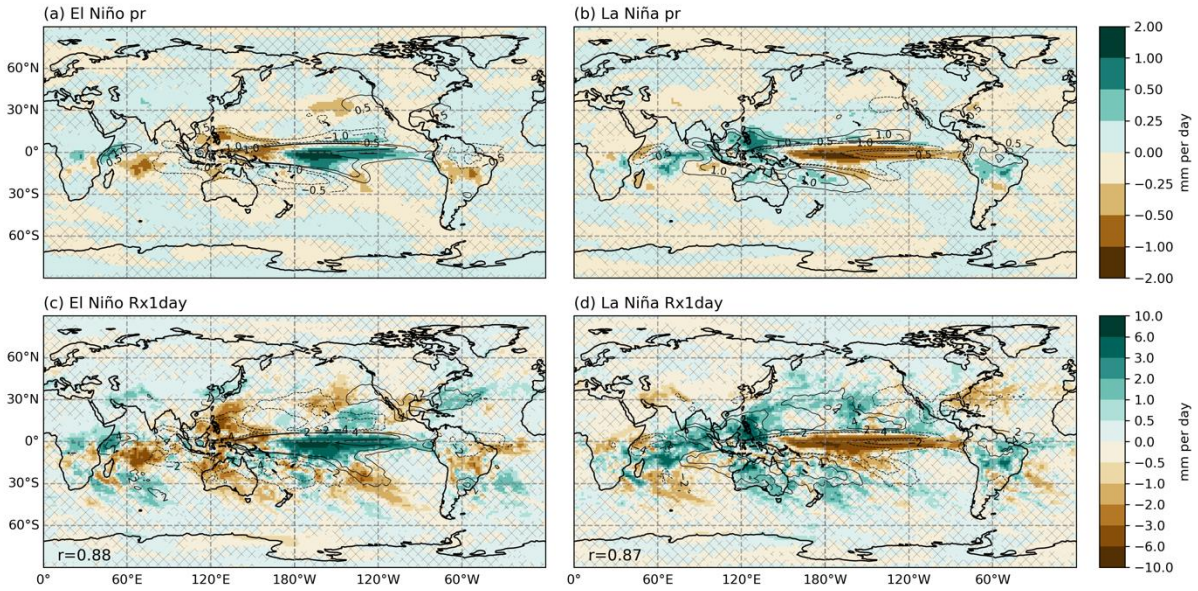

Figure 8: CMIP6 multi model mean composites of change in DJF seasonal mean and extreme precipitation during El Niño and La Niña events under SSP5-8.5 in mm/day. Change is future composite (2015-2100) relative to the historical composite (1900-2014). Panels depict a) El Niño pr b) La Niña pr c) El Niño Rx1day d) La Niña Rx1day. R value in bottom left of extreme composite represent pattern correlation with mean composite. Contours depict historical teleconnection.

Next, the percentage of land area that experiences a change in the magnitude of the ENSO teleconnection anomalies under SSP5-8.5 for ts, pr, TXx, TNn, and Rx1day is examined. This is done by taking the spatial changes shown in Figure 7 and 8 and calculating the change in the anomaly at each land grid point as a percentage relative to the magnitude of the historical anomaly. A change in magnitude in the same direction as the historical anomaly is defined as an amplification and a change in magnitude in the opposite direction as a dampening. The fraction of land which shows an amplification for a range of magnitudes is shown in Figure 9.

Accepted for publication in *Journal of Climate.* DOI 10.1175/JCLI-D-23-0619.1

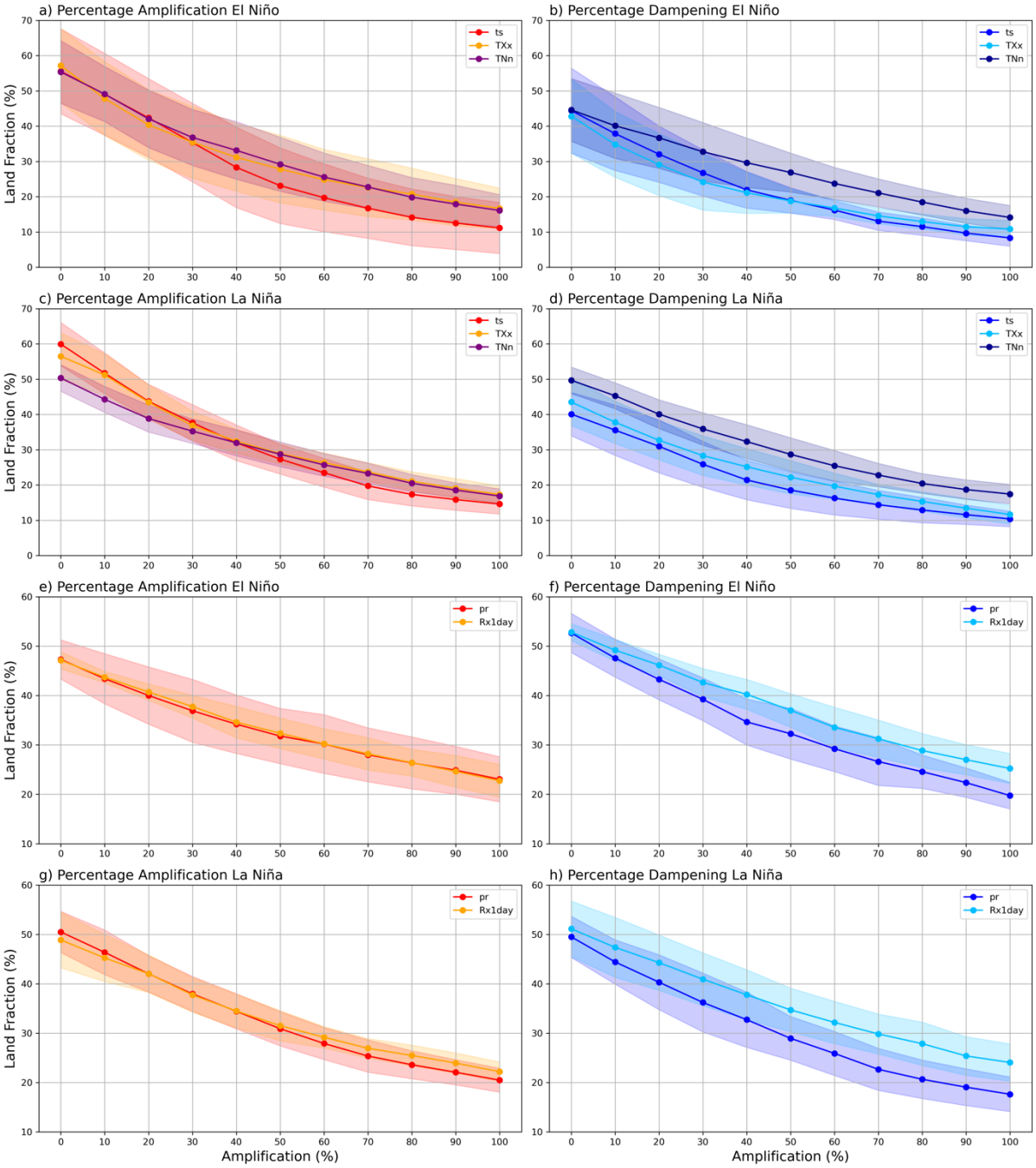

Figure 9: Scatter plots depicting the proportion of land area that experiences an amplification (left) and dampening (right) of El Niño and La Niña teleconnections under SSP5-8.5 across distinct magnitudes. The magnitude indicates the percentage that the teleconnection strengthens. Panels depict the percentage of land area with amplified (or dampened) teleconnections for seasonal DJF a), b) ts, Txx, and Tnn during El Niño events c), d) ts, TXx, and TNn during La Niña events e), f) pr and Rx1day during El Niño events g), h) pr and Rx1day during La Niña events. The line represents the multi-model median, while the shading indicates the model spread (interquartile range).

We only consider land that shows a significant teleconnection with ENSO (correlation > |0.2|) in the historical period in Figure 9 and grid points that do not satisfy this criterion are discarded. Testing was conducted to identify regions that may experience a strengthening

Accepted for publication in *Journal of Climate*. DOI 10.1175/JCLI-D-23-0619.1

from below 0.2 in the historical period to above 0.2 in the future period, however this did not impact results. When looking at the ensemble mean, ~55% of the global land area that is influenced by ENSO shows an amplification of the temperature teleconnection in El Niño in the future period under SSP5-8.5 (Figure 9a). An amplification in this case applies to both positive and negative anomalies meaning that warm anomalies get warmer or cold anomalies get colder. These results indicate that mean temperature anomalies during El Niño will become larger in just over half of the regions that already experience significant anomalies during El Niño. Around 30% of the land area impacted by ENSO will see an amplification of 50% and around 15% of the land area will see a doubling of the mean temperature anomalies experienced during El Niño. The same is broadly true for La Niña with ~50-60% of regions experiencing any amplification and ~15-20% experiencing a doubling in the magnitude of the anomalies (Figure 9c).

These results suggest that the La Niña teleconnection with mean temperatures amplifies slightly more than for El Niño, especially for the larger amplitude changes. As for TXx and TNn, they compare very closely for the El Niño case, but in the case of La Niña they deviate from each other at the lower end of the amplitude changes before converging at the higher end. The amplification of temperature extremes broadly scales at an equivalent rate to the mean, but with larger changes for El Niño. This implies that regions that are projected to experience an amplification of the ENSO teleconnection under future warming can also expect a comparable amplification in the intensity of extremes. We note that the area of land that experiences an amplification in extreme temperatures during El Niño is ~5% larger than the area that experiences an amplification in mean temperatures based on the multi model median. However, it is worth noting that the model spread in the El Niño amplification is also larger than for La Niña (see Figure 9a and c). The percentage dampening was also examined, and results show that the mean temperature teleconnection dampens slightly more for El Niño than La Niña at the lowest amplification level, but similarly for higher thresholds (Figure 9b and d). For the extremes, TNn dampens more for La Niña and TXx dampens consistently across phases.

When assessing mean rainfall anomalies due to ENSO in a future warmer climate, we find that around 45-50% of the global landmass with significant ENSO influence experiences an amplification and ~20% experiences a doubling in the size of the anomalies (Figure 9e and

Accepted for publication in *Journal of Climate.* DOI 10.1175/JCLI-D-23-0619.1

g). This is true for El Niño and La Niña anomalies. The Rx1day anomalies have a very similar response to the mean for both El Niño and La Niña. There is a smaller spread across the models for precipitation and Rx1day changes than for mean temperature and the temperature extremes when using interquartile range (IQR) as a measure of spread (IQR = 24% and 12% for ts for El Niño and La Niña respectively and IQR = 8% for pr for both El Niño and La Niña). This amplification of the mean ENSO temperature and precipitation teleconnections is consistent with the amplification found by McGregor et al. (2022). Here we have shown that a similar amplification also applies to ENSO teleconnections with temperature and precipitation extremes. When considering dampening, Pr and Rx1day dampen for a similar land fraction at lower amplification levels but diverge as amplification rate increases, with Rx1day dampening in ~5% more land regions than mean precipitation (Figure 9f and h). This is consistent for El Niño and La Niña, and both the mean and extreme dampen slightly more for El Niño.

c. Mechanisms for projected changes in ENSO teleconnections

To see if models with higher ENSO variability are projecting greater teleconnection amplification, we correlate the percentage of land that experiences an amplification of the teleconnection in each model with its change in ENSO amplitude (Figure 10), as ENSO amplitude changes have been previously shown to greatly influence results (Stevenson et al., 2021). Change in ENSO amplitude is defined as the change in standard deviation of the Niño34 index in the future period compared to the historical period. We find a moderate-strong correlation between SST variability in the NINO3.4 region with the amplification of precipitation variables (pr and Rx1day). The correlation is stronger for the extreme Rx1day rainfall than mean precipitation (r = 0.65 for Rx1day and 0.61 for mean precipitation for La Niña). The correlation is similar for El Niño (r = 0.63 for Rx1day and r = 0.56 for mean precipitation). This suggests that the rainfall amplification increases with increased ENSO amplitude for both La Niña and El Niño events, however slightly more for La Niña. ENSO amplitude also correlates strongly with temperature for La Niña however, the correlation is strongest in the mean rather than the extremes (see Supplementary Figure S9, r = 0.8 for ts, r = 0.74 for TXx, r = 0.65 for TNn). There is also strong correlation between mean and extreme temperature and ENSO amplitude for El Niño (see Supplementary Figure S9, r=0.69 for ts, r=0.7 for TXx, and r=0.61 for TNn). To test sensitivity of results to choice of ensemble

Accepted for publication in *Journal of Climate.* DOI 10.1175/JCLI-D-23-0619.1

member, we repeated these results in the CanESM5 and the MPI-ESM-2-LR large ensembles (Figure S10, S11, S12, S13) and found negligible impact. These findings are consistent with Bonfils et al. (2015), who found that while precipitation variability intensifies even in the absence of ENSO amplitude changes, ENSO SST variability modulates the amplification of precipitation variability and is largest in models that project increased ENSO amplitude.

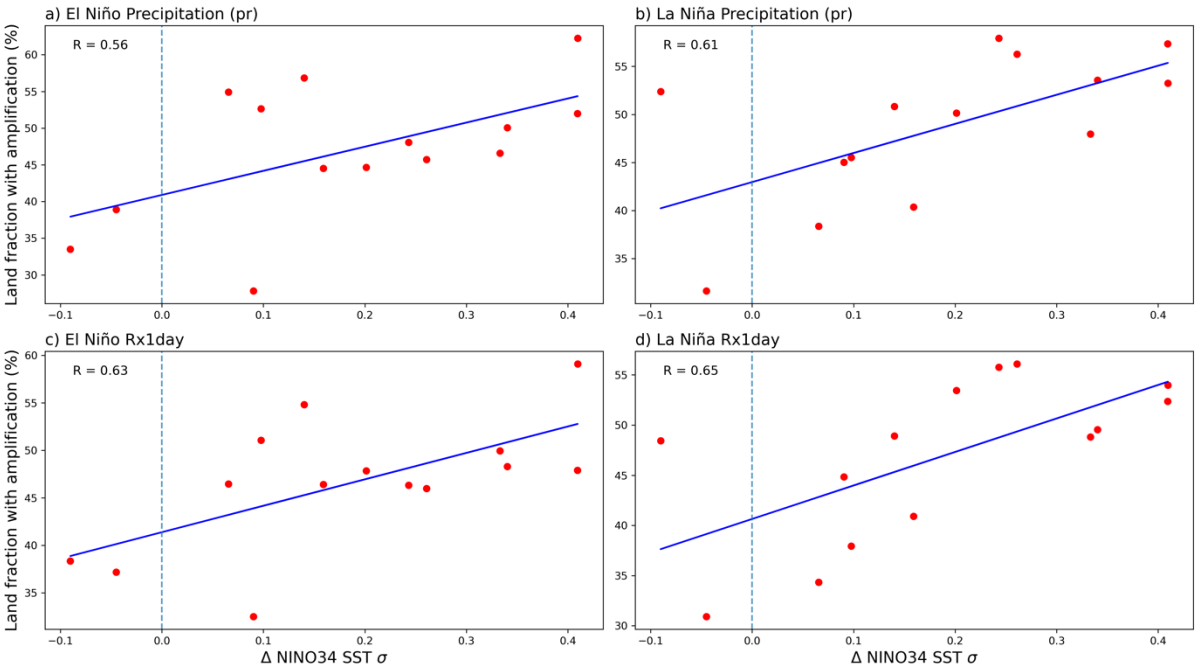

Figure 10: Scatter plots illustrating the relationship between the percentage of land area experiencing any teleconnection amplification and the change in ENSO amplitude across all models. Each panel depicts the percentage of land area with amplified teleconnections against the change in ENSO amplitude for seasonal DJF a) pr during El Niño events b) pr during La Niña events c) Rx1day during El Niño events d) Rx1day during La Niña events.

4. Summary and Conclusion

We have demonstrated that there is a teleconnection between ENSO and extreme temperature and precipitation in the historical period using 20CRv3 reanalysis. The spatial patterns of these teleconnections are similar, but not identical, to the spatial patterns of the ENSO teleconnection with mean temperature and precipitation. Like the mean, the ENSO influence on extremes is greatest in Australia, South Africa, and parts of North and South America. Regions where the sign of the extreme cold temperature teleconnection pattern differs from the mean temperature teleconnection pattern include southeast Australia and Central America. The sign of the extreme precipitation teleconnection agrees with the sign of the mean precipitation pattern in most regions.

Accepted for publication in *Journal of Climate*. DOI 10.1175/JCLI-D-23-0619.1

The CMIP6 models broadly capture the spatial pattern of rainfall (with pattern correlation values in the range of 0.5 to 0.8) however, the multi model mean overestimates or underestimates the magnitude of the anomalies in some regions (such as in parts of the Maritime Continent, South Africa, northern South America, and Australia) compared to the reanalysis. The models generally do not do as well at capturing the spatial pattern of temperature. Errors in the model's teleconnections may arise from biases in the representation of general circulation as well as biases in the tropical Pacific such as the cold tongue bias, and the difficulty of simulating the correct ENSO pattern and location which are known to be important for simulating teleconnections (Bayr et al., 2018; Planton et al., 2021).

We have demonstrated here that ENSO influences extreme temperature and precipitation globally. Our findings are in agreement with the previous findings of Kenyon and Hegerl (2008) and Kenyon and Hegerl (2010) with added global coverage. The teleconnection to extremes for both El Niño and La Niña is generally spatially similar to the teleconnection with mean temperature and precipitation, with some regional differences found mainly in the case of the extreme cold nights. The CMIP6 models are able to simulate the sign of the anomalies in the mean case and the extreme case, in agreement with the reanalysis.

Under high emissions, the amplification of the El Niño and La Niña teleconnection found in the mean climate is also found for extremes and is slightly larger for extreme temperatures during El Niño. Under SSP5-8.5, the models suggest that we may see an amplification of the anomalies associated with El Niño and La Niña for ts, TXx, TNn, pr, and Rx1day. The CMIP6 models show an amplification in the magnitude of the anomalies in around ~50% of regions and doubling in ~20% of regions globally. This could have devastating consequences for regions that already experience damaging extreme events under El Niño and La Niña events. This amplification in the ENSO impact will be experienced in addition to mean state climate change impacts. As extreme precipitation is predicted to intensify generally, ENSO may further enhance this. The same is true for extreme temperatures, which are expected to intensify as the climate warms (Ajjur & Al-Ghamdi, 2021; Li et al., 2021; Sillmann et al., 2013).

Accepted for publication in *Journal of Climate.* DOI 10.1175/JCLI-D-23-0619.1

Analysis of future changes in ENSO teleconnections relies on CMIP6 models. It is worth noting that models continue to have systematic biases in their simulation of ENSO and teleconnection patterns (Planton et al., 2021). In addition, there is continued disagreement regarding future changes in ENSO amplitude and spatial pattern (Beobide-Arsuaga et al., 2021). Model trends in tropical Pacific SSTs and associated Walker Circulation strength also disagree with historical trends (Heede & Fedorov, 2023). Therefore, it is important to consider these uncertainties when examining changes in ENSO teleconnections in CMIP6 models. We find that the amplification of teleconnections is correlated with the changes in ENSO amplitude (Figure 10). As models disagree on the sign and magnitude of changes in ENSO amplitude, this implies uncertainty in the magnitude of increased teleconnections. However, we find that all models simulate strengthened teleconnections regardless of whether ENSO becomes stronger, consistent with Fasullo et al. (2018) and Bonfils et al. (2015).

Previous work has shown that mean ENSO teleconnection amplification scales with the magnitude of the warming i.e., SSP5-8.5 leads to the largest and most widespread changes as it is the warmest of the SSP scenarios (McGregor et al., 2022). Unfortunately, data for the extreme indices was not available at the time of this study under each of the SSP scenarios but investigating teleconnection changes with extremes for a range of SSP scenarios should be considered in future work. Our analysis finds changes to ENSO teleconnections with extremes under continued global warming. Given the impacts of ENSO-associated extremes, particularly in more vulnerable regions (Lieber et al., 2022), this is one of many incentives to limit global warming through reduced greenhouse gas emissions.

Acknowledgements.

The authors would like to acknowledge the World Climate Research Programme, which, through its Working Group on Coupled Modelling, coordinated and promoted CMIP6 and thank the climate modelling groups for producing and making their data available for use. Support for the Twentieth Century Reanalysis Project version 3 dataset is provided by the U.S. Department of Energy, Office of Science Biological and Environmental Research (BER), by the National Oceanic and Atmospheric Administration Climate Program Office, and by the NOAA Physical Sciences Laboratory. This research was supported by the Australian Research Council (ARC) Centre of Excellence for Climate Extremes and the

National Computational Infrastructure at the Australian National University. The work of RL was funded by an Australian Government Research Training Program (RTP) Scholarship. RL, JB, and AK were supported by ARC Grant CE170100023. JB and AK acknowledge support from the Australian Government's National Environmental Science Program Climate Systems Hub.

Data availability statement.

All data is publicly available and can be downloaded from the following URLs.

CMIP6: https://esgf-node.llnl.gov/search/cmip6/

20CRv3: https://portal.nersc.gov/project/20C_Reanalysis/

HadISST: https://www.metoffice.gov.uk/hadobs/hadisst/data/download.html

ETCCDI indices: https://cds.climate.copernicus.eu/cdsapp#!/dataset/sis-extreme-indices-cmip6?tab=overview

REFERENCES

Ajjur, S. B., & Al-Ghamdi, S. G. (2021). Global hotspots for future absolute temperature extremes from CMIP6 models. *Earth and Space Science*, *8*(9), e2021EA001817.

Alexander, L. V., Zhang, X., Peterson, T. C., Caesar, J., Gleason, B., Tank, A. M. G. K., Haylock, M., Collins, D., Trewin, B., Rahimzadeh, F., Tagipour, A., Kumar, K. R., Revadekar, J., Griffiths, G., Vincent, L., Stephenson, D. B., Burn, J., Aguilar, E., Brunet, M., . . . Vazquez-Aguirre, J. L. (2006). Global observed changes in daily climate extremes of temperature and precipitation. *Journal of Geophysical Research-Atmospheres*, *111*(D5). https://doi.org/10.1029/2005jd006290

Allen, R. J., & Anderson, R. G. (2018). 21st century California drought risk linked to model fidelity of the El Niño teleconnection. *NPJ Climate and Atmospheric Science*, *1*(1), 21.

Anderson, W., Seager, R., Baethgen, W., Cane, M., & You, L. (2019). Synchronous crop failures and climate-forced production variability. *Science advances*, *5*(7), eaaw1976.

Arblaster, J. M., & Alexander, L. V. (2012). The impact of the El Nino-Southern Oscillation on maximum temperature extremes. *Geophysical Research Letters*, *39*. https://doi.org/10.1029/2012gl053409

Avila, F. B., Dong, S., Menang, K. P., Rajczak, J., Renom, M., Donat, M. G., & Alexander, L. V. (2015). Systematic investigation of gridding-related scaling effects on annual statistics of daily temperature and precipitation maxima: A case study for south-east Australia. *Weather and Climate Extremes*, *9*, 6-16. https://doi.org/https://doi.org/10.1016/j.wace.2015.06.003

Bayr, T., Latif, M., Dommenget, D., Wengel, C., Harlaß, J., & Park, W. (2018). Mean-state dependence of ENSO atmospheric feedbacks in climate models. *Climate Dynamics*, *50*, 3171-3194.

Bellenger, H., Guilyardi, E., Leloup, J., Lengaigne, M., & Vialard, J. (2014). ENSO representation in climate models: From CMIP3 to CMIP5. *Climate Dynamics*, *42*, 1999-2018.

Beobide-Arsuaga, G., Bayr, T., Reintges, A., & Latif, M. (2021). Uncertainty of ENSO-amplitude projections in CMIP5 and CMIP6 models. *Climate Dynamics*. https://doi.org/10.1007/s00382-021-05673-4

Beverley, J. D., Collins, M., Lambert, F. H., & Chadwick, R. (2021). Future changes to El Niño teleconnections over the north Pacific and North America. *Journal of Climate*, *34*(15), 6191-6205.

Bonfils, C. J. W., Santer, B. D., Phillips, T. J., Marvel, K., Leung, L. R., Doutriaux, C., & Capotondi, A. (2015). Relative Contributions of Mean-State Shifts and ENSO-Driven Variability to Precipitation Changes in a Warming Climate. *Journal of Climate*, *28*(24), 9997-10013. https://doi.org/10.1175/Jcli-D-15-0341.1

Burgers, G., & Stephenson, D. B. (1999). The "normality" of el niño. *Geophysical Research Letters*, *26*(8), 1027-1030.

Cai, W., Ng, B., Wang, G., Santoso, A., Wu, L., & Yang, K. (2022). Increased ENSO sea surface temperature variability under four IPCC emission scenarios. *Nature Climate Change*, *12*(3), 228-231.

Cai, W. J., McPhaden, M. J., Grimm, A. M., Rodrigues, R. R., Taschetto, A. S., Garreaud, R. D., Dewitte, B., Poveda, G., Ham, Y. G., Santoso, A., Ng, B., Anderson, W., Wang, G. J., Geng, T., Jo, H. S., Marengo, J. A., Alves, L. M., Osman, M., Li, S. J., . . . Vera, C. (2020). Climate impacts of the El Nino-Southern Oscillation on South America. *Nature Reviews Earth & Environment*, *1*(4), 215-231. https://doi.org/10.1038/s43017-020-0040-3

Callahan, C. W., & Mankin, J. S. (2023). Persistent effect of El Niño on global economic growth. *Science*, *380*(6649), 1064-1069. https://doi.org/doi:10.1126/science.adf2983

Accepted for publication in *Journal of Climate*. DOI 10.1175/JCLI-D-23-0619.1

Cayan, D. R., Redmond, K. T., & Riddle, L. G. (1999). ENSO and hydrologic extremes in the western United States. *Journal of Climate*, *12*(9), 2881-2893.

Chen, C., Sahany, S., Moise, A. F., Chua, X. R., Hassim, M. E., Lim, G., & Prasanna, V. (2023). ENSO–Rainfall Teleconnection over the Maritime Continent Enhances and Shifts Eastward under Warming. *Journal of Climate*, *36*(14), 4635-4663.

Chen, L.-C., Van den Dool, H., Becker, E., & Zhang, Q. (2017). ENSO precipitation and temperature forecasts in the North American Multimodel Ensemble: Composite analysis and validation. *Journal of Climate*, *30*(3), 1103-1125.

Chung, C., Boschat, G., Taschetto, A., Narsey, S., McGregor, S., Santoso, A., & Delage, F. (2023). Evaluation of seasonal teleconnections to remote drivers of Australian rainfall in CMIP5 and CMIP6 models. *Journal of Southern Hemisphere Earth Systems Science*.

Chung, C. T. Y., & Power, S. B. (2017). The non-linear impact of El Nino, La Nina and the Southern Oscillation on seasonal and regional Australian precipitation. *Journal of Southern Hemisphere Earth Systems Science*, *67*(1), 25-45. https://doi.org/https://doi.org/10.1071/ES17004

Compo, G. P., Whitaker, J. S., Sardeshmukh, P. D., Matsui, N., Allan, R. J., Yin, X., Gleason, B. E., Vose, R. S., Rutledge, G., Bessemoulin, P., Bronnimann, S., Brunet, M., Crouthamel, R. I., Grant, A. N., Groisman, P. Y., Jones, P. D., Kruk, M. C., Kruger, A. C., Marshall, G. J., . . . Worley, S. J. (2011). The Twentieth Century Reanalysis Project. *Quarterly Journal of the Royal Meteorological Society*, *137*(654), 1-28. https://doi.org/10.1002/qj.776

Costa, M. D., Oliveira, J. F. D., dos Santos, P. J., Correia, W. L. F., de Gois, G., Blanco, C. J. C., Teodoro, P. E., da Silva, C. A., Santiago, D. D., Souza, E. D., & Jardim, A. M. D. F. (2021). Rainfall extremes and drought in Northeast Brazil and its relationship with El Nino-Southern Oscillation. *International Journal of Climatology*, *41*, E2111-E2135. https://doi.org/10.1002/joc.6835

Crimp, S., Bakar, K. S., Kokic, P., Jin, H., Nicholls, N., & Howden, M. (2015). Bayesian space–time model to analyse frost risk for agriculture in Southeast Australia. *International Journal of Climatology*, *35*(8), 2092-2108.

Donat, M. G., Alexander, L. V., Herold, N., & Dittus, A. J. (2016). Temperature and precipitation extremes in century-long gridded observations, reanalyses, and atmospheric model simulations. *Journal of Geophysical Research-Atmospheres*, *121*(19), 11174-11189. https://doi.org/10.1002/2016jd025480

Accepted for publication in *Journal of Climate*. DOI 10.1175/JCLI-D-23-0619.1

Donat, M. G., Peterson, T. C., Brunet, M., King, A. D., Almazroui, M., Kolli, R. K., Boucherf, D., Al-Mulla, A. Y., Nour, A. Y., Aly, A. A., Nada, T. A. A., Semawi, M. M., Dashti, H. A., Salhab, T. G., Fadli, K. I., Muftah, M. K., Eida, S. D., Badi, W., Driouech, F., . . . Al Shekaili, M. N. (2014). Changes in extreme temperature and precipitation in the Arab region: long-term trends and variability related to ENSO and NAO. *International Journal of Climatology*, *34*(3), 581-592. https://doi.org/10.1002/joc.3707

Dunn, R. J., Donat, M. G., & Alexander, L. V. (2022). Comparing extremes indices in recent observational and reanalysis products. *Frontiers in Climate*, *4*, 989505.

Dunn, R. J. H., Alexander, L. V., Donat, M. G., Zhang, X. B., Bador, M., Herold, N., Lippmann, T., Allan, R., Aguilar, E., Barry, A. A., Brunet, M., Caesar, J., Chagnaud, G., Cheng, V., Cinco, T., Durre, I., de Guzman, R., Htay, T. M., Ibadullah, W. M. W., . . . Yussof, M. N. B. (2020). Development of an Updated Global Land In Situ-Based Data Set of Temperature and Precipitation Extremes: HadEX3. *Journal of Geophysical Research-Atmospheres*, *125*(16). https://doi.org/https://doi.org/10.1029/2019JD032263

Eyring, V., Bony, S., Meehl, G. A., Senior, C. A., Stevens, B., Stouffer, R. J., & Taylor, K. E. (2016). Overview of the Coupled Model Intercomparison Project Phase 6 (CMIP6) experimental design and organization. *Geoscientific Model Development*, *9*(5), 1937-1958. https://doi.org/10.5194/gmd-9-1937-2016

Fasullo, J. T., Otto-Bliesner, B. L., & Stevenson, S. (2018). ENSO's Changing Influence on Temperature, Precipitation, and Wildfire in a Warming Climate. *Geophysical Research Letters*, *45*(17), 9216-9225. https://doi.org/10.1029/2018gl079022

Feng, T., Zhu, X., & Dong, W. (2023). Historical assessment and future projection of extreme precipitation in CMIP6 models: Global and continental. *International Journal of Climatology*.

Frauen, C., Dommenget, D., Tyrrell, N., Rezny, M., & Wales, S. (2014). Analysis of the Nonlinearity of El Nino-Southern Oscillation Teleconnections. *Journal of Climate*, *27*(16), 6225-6244. https://doi.org/10.1175/Jcli-D-13-00757.1

Freund, M. B., Brown, J. R., Henley, B. J., Karoly, D. J., & Brown, J. N. (2020). Warming Patterns Affect El Nino Diversity in CMIP5 and CMIP6 Models. *Journal of Climate*, *33*(19), 8237-8260. https://doi.org/10.1175/Jcli-D-19-0890.1

Freund, M. B., Marshall, A. G., Wheeler, M. C., & Brown, J. N. (2021). Central Pacific El Nino as a Precursor to Summer Drought-Breaking Rainfall Over Southeastern

Accepted for publication in *Journal of Climate*. DOI 10.1175/JCLI-D-23-0619.1

Australia. *Geophysical Research Letters*, *48*(7). https://doi.org/10.1029/2020GL091131

Gershunov, A., & Barnett, T. P. (1998). ENSO influence on intraseasonal extreme rainfall and temperature frequencies in the contiguous United States: Observations and model results. *Journal of Climate*, *11*(7), 1575-1586.

Goddard, L., & Gershunov, A. (2020). Impact of El Niño on Weather and Climate Extremes. *El Niño Southern Oscillation in a Changing Climate*, 361-375.

Grimm, A. M., Almeida, A. S., Beneti, C. A. A., & Leite, E. A. (2020). The combined effect of climate oscillations in producing extremes: the 2020 drought in southern Brazil. *Rbrh-Revista Brasileira De Recursos Hidricos*, *25*. https://doi.org/ARTN e48 10.1590/2318-0331.252020200116

Grimm, A. M., & Tedeschi, R. G. (2009). ENSO and Extreme Rainfall Events in South America. *Journal of Climate*, *22*(7), 1589-1609. https://doi.org/10.1175/2008jcli2429.1

Grose, M. R., Narsey, S., Delage, F. P., Dowdy, A. J., Bador, M., Boschat, G., Chung, C., Kajtar, J. B., Rauniyar, S., Freund, M. B., Lyu, K., Rashid, H., Zhang, X., Wales, S., Trenham, C., Holbrook, N. J., Cowan, T., Alexander, L., Arblaster, J. M., & Power, S. (2020). Insights From CMIP6 for Australia's Future Climate. *Earths Future*, *8*(5). https://doi.org/10.1029/2019EF001469

Hao, Z. C., Hao, F. H., Singh, V. P., & Zhang, X. (2018). Quantifying the relationship between compound dry and hot events and El Nino-southern Oscillation (ENSO) at the global scale. *Journal of Hydrology*, *567*, 332-338. https://doi.org/10.1016/j.jhydrol.2018.10.022

Hausfather, Z., & Peters, G. P. (2020). Emissions–the 'business as usual'story is misleading. *Nature*, *577*(7792), 618-620.

Heede, U. K., & Fedorov, A. V. (2023). Colder eastern equatorial Pacific and stronger Walker circulation in the early 21st century: separating the forced response to global warming from natural variability. *Geophysical Research Letters*, *50*(3), e2022GL101020.

Huang, X., & Stevenson, S. (2023). Contributions of Climate Change and ENSO Variability to Future Precipitation Extremes Over California. *Geophysical Research Letters*, *50*(12), e2023GL103322. https://doi.org/https://doi.org/10.1029/2023GL103322

Jiang, W., Huang, P., Huang, G., & Ying, J. (2021). Origins of the excessive westward extension of ENSO SST simulated in CMIP5 and CMIP6 models. *Journal of Climate*, *34*(8), 2839-2851.

Accepted for publication in *Journal of Climate*. DOI 10.1175/JCLI-D-23-0619.1

Jimenez-Munoz, J. C., Mattar, C., Barichivich, J., Santamaria-Artigas, A., Takahashi, K., Malhi, Y., Sobrino, J. A., & van der Schrier, G. (2016). Record-breaking warming and extreme drought in the Amazon rainforest during the course of El Nino 2015-2016. *Scientific Reports*, *6*. https://doi.org/ARTN 33130
10.1038/srep33130

Jones, D. A., & Trewin, B. C. (2000). On the relationships between the El Nino-Southern Oscillation and Australian land surface temperature. *International Journal of Climatology*, *20*(7), 697-719. https://doi.org/10.1002/1097-0088(20000615)20:7<697::Aid-Joc499>3.0.Co;2-A

Kenyon, J., & Hegerl, G. C. (2008). Influence of modes of climate variability on global temperature extremes. *Journal of Climate*, *21*(15), 3872-3889. https://doi.org/10.1175/2008jcli2125.1

Kenyon, J., & Hegerl, G. C. (2010). Influence of Modes of Climate Variability on Global Precipitation Extremes. *Journal of Climate*, *23*(23), 6248-6262. https://doi.org/10.1175/2010jcli3617.1

Kim, Y.-H., Min, S.-K., Zhang, X., Sillmann, J., & Sandstad, M. (2020). Evaluation of the CMIP6 multi-model ensemble for climate extreme indices. *Weather and Climate Extremes*, *29*, 100269.

Kirchmeier-Young, M. C., & Zhang, X. (2020). Human influence has intensified extreme precipitation in North America. *Proceedings of the National Academy of Sciences*, *117*(24), 13308-13313.

Li, C., Zwiers, F., Zhang, X., Li, G., Sun, Y., & Wehner, M. (2021). Changes in annual extremes of daily temperature and precipitation in CMIP6 models. *Journal of Climate*, *34*(9), 3441-3460.

Li, G., & Xie, S.-P. (2014). Tropical biases in CMIP5 multimodel ensemble: The excessive equatorial Pacific cold tongue and double ITCZ problems. *Journal of Climate*, *27*(4), 1765-1780.

Lieber, R., King, A., Brown, J., Ashcroft, L., Freund, M., & McMichael, C. (2022). ENSO teleconnections more uncertain in regions of lower socioeconomic development. *Geophysical Research Letters*, *49*(21), e2022GL100553.

Luo, M., & Lau, N. C. (2019). Amplifying effect of ENSO on heat waves in China. *Climate Dynamics*, *52*(5-6), 3277-3289. https://doi.org/10.1007/s00382-018-4322-0

Accepted for publication in *Journal of Climate*. DOI 10.1175/JCLI-D-23-0619.1

Luo, M., & Lau, N. C. (2020). Summer heat extremes in northern continents linked to developing ENSO events. *Environmental Research Letters*, *15*(7). https://doi.org/ARTN 074042
10.1088/1748-9326/ab7d07

Lyon, B. (2004). The strength of El Nino and the spatial extent of tropical drought. *Geophysical Research Letters*, *31*(21). https://doi.org/10.1029/2004gl020901

McGregor, S., Cassou, C., Kosaka, Y., & Phillips, A. S. (2022). Projected ENSO teleconnection changes in CMIP6. *Geophysical Research Letters*, *49*(11), e2021GL097511.

McPhaden, M. J., Zebiak, S. E., & Glantz, M. H. (2006). ENSO as an integrating concept in Earth science. *Science*, *314*(5806), 1740-1745. https://doi.org/10.1126/science.1132588

Meque, A., & Abiodun, B. J. (2015). Simulating the link between ENSO and summer drought in Southern Africa using regional climate models. *Climate Dynamics*, *44*(7-8), 1881-1900. https://doi.org/10.1007/s00382-014-2143-3

Min, S.-K., Cai, W., & Whetton, P. (2013). Influence of climate variability on seasonal extremes over Australia. *Journal of Geophysical Research: Atmospheres*, *118*(2), 643-654. https://doi.org/https://doi.org/10.1002/jgrd.50164

Min, S.-K., Zhang, X., Zwiers, F. W., & Hegerl, G. C. (2011). Human contribution to more-intense precipitation extremes. *Nature*, *470*(7334), 378-381.

Mo, K. C., & Schemm, J. E. (2008). Relationships between ENSO and drought over the southeastern United States. *Geophysical Research Letters*, *35*(15). https://doi.org/Artn L15701
10.1029/2008gl034656

Müller, G. V., Nuñez, M. N., & Seluchi, M. E. (2000). Relationship between ENSO cycles and frost events within the Pampa Húmeda region. *International Journal of Climatology: A Journal of the Royal Meteorological Society*, *20*(13), 1619-1637.

O'Neill, B. C., Tebaldi, C., Van Vuuren, D. P., Eyring, V., Friedlingstein, P., Hurtt, G., Knutti, R., Kriegler, E., Lamarque, J.-F., & Lowe, J. (2016). The scenario model intercomparison project (ScenarioMIP) for CMIP6. *Geoscientific Model Development*, *9*(9), 3461-3482.

Perry, S., McGregor, S., Sen Gupta, A., England, M., & Maher, N. (2020). Projected late 21st century changes to the regional impacts of the El Niño-Southern Oscillation. *Climate Dynamics*, *54*, 395-412.

Accepted for publication in *Journal of Climate*. DOI 10.1175/JCLI-D-23-0619.1

Perry, S. J., McGregor, S., Gupta, A. S., & England, M. H. (2017). Future changes to El Niño–Southern Oscillation temperature and precipitation teleconnections. *Geophysical Research Letters*, *44*(20), 10,608-610,616.

Planton, Y. Y., Guilyardi, E., Wittenberg, A. T., Lee, J., Gleckler, P. J., Bayr, T., McGregor, S., McPhaden, M. J., Power, S., & Roehrig, R. (2021). Evaluating climate models with the CLIVAR 2020 ENSO metrics package. *Bulletin of the American Meteorological Society*, *102*(2), E193-E217.

Power, S., Delage, F., Chung, C., Kociuba, G., & Keay, K. (2013). Robust twenty-first-century projections of El Nino and related precipitation variability. *Nature*, *502*(7472), 541-+. https://doi.org/10.1038/nature12580

Power, S., Haylock, M., Colman, R., & Wang, X. (2006). The predictability of interdecadal changes in ENSO activity and ENSO teleconnections. *Journal of Climate*, *19*(19), 4755-4771.

Rayner, N., Parker, D. E., Horton, E., Folland, C. K., Alexander, L. V., Rowell, D., Kent, E. C., & Kaplan, A. (2003). Global analyses of sea surface temperature, sea ice, and night marine air temperature since the late nineteenth century. *Journal of Geophysical Research: Atmospheres*, *108*(D14).

Rifai, S. W., Li, S., & Malhi, Y. (2019). Coupling of El Nino events and long-term warming leads to pervasive climate extremes in the terrestrial tropics. *Environmental Research Letters*, *14*(10). https://doi.org/ARTN 105002
10.1088/1748-9326/ab402f

Ropelewski, C. F., & Halpert, M. S. (1987). Global and Regional Scale Precipitation Patterns Associated with the El-Nino Southern Oscillation. *Monthly Weather Review*, *115*(8), 1606-1626. https://doi.org/10.1175/1520-0493(1987)115<1606:Garspp>2.0.Co;2

Rusticucci, M., Barrucand, M., & Collazo, S. (2017). Temperature extremes in the Argentina central region and their monthly relationship with the mean circulation and ENSO phases. *International Journal of Climatology*, *37*(6), 3003-3017. https://doi.org/10.1002/joc.4895

Sandstad, M., Schwingshackl, C., & Iles, C. (2022). *Climate extreme indices and heat stress indicators derived from CMIP6 global climate projections. Copernicus Climate Change Service (C3S) Climate Data Store (CDS).* https://doi.org/10.24381/cds.776e08bd

Seneviratne, S. I., Zhang, X., Adnan, M., Badi, W., Dereczynski, C., Di Luca, A., Ghosh, S., Iskandar, I., Kossin, J., Lewis, S., Otto, F., Pinto, I., Satoh, M., Vicente-Serrano, S.

Accepted for publication in *Journal of Climate*. DOI 10.1175/JCLI-D-23-0619.1

M., Wehner, M., & Zhou, B. (2021). Weather and Climate Extreme Events in a Changing Climate. In Climate Change 2021: The Physical Science Basis. Contribution of Working Group I to the Sixth Assessment Report of the Intergovernmental Panel on Climate Change[Masson-Delmotte, V., P. Zhai, A. Pirani, S.L. Connors, C. Péan, S. Berger, N. Caud, Y. Chen, L. Goldfarb, M.I. Gomis, M. Huang, K. Leitzell, E. Lonnoy, J.B.R. Matthews, T.K. Maycock, T. Waterfield, O. Yelekçi, R. Yu, and B. Zhou (eds.)]. Cambridge University Press, Cambridge, United Kingdom and New York, NY, USA, pp. 1513–1766. https://doi.org/**10.1017/9781009157896.013**

Sillmann, J., Kharin, V. V., Zwiers, F. W., Zhang, X., & Bronaugh, D. (2013). Climate extremes indices in the CMIP5 multimodel ensemble: Part 2. Future climate projections. *Journal of Geophysical Research-Atmospheres*, *118*(6), 2473-2493. https://doi.org/10.1002/jgrd.50188

Slivinski, L. C., Compo, G. P., Sardeshmukh, P. D., Whitaker, J. S., McColl, C., Allan, R. J., Brohan, P., Yin, X., Smith, C. A., Spencer, L. J., Vose, R. S., Rohrer, M., Conroy, R. P., Schuster, D. C., Kennedy, J. J., Ashcroft, L., Bronnimann, S., Brunet, M., Camuffo, D., . . . Wood, K. (2021). An Evaluation of the Performance of the Twentieth Century Reanalysis Version 3. *Journal of Climate*, *34*(4), 1417-1438. https://doi.org/10.1175/Jcli-D-20-0505.1

Slivinski, L. C., Compo, G. P., Whitaker, J. S., Sardeshmukh, P. D., Giese, B. S., McColl, C., Allan, R., Yin, X. G., Vose, R., Titchner, H., Kennedy, J., Spencer, L. J., Ashcroft, L., Bronnimann, S., Brunet, M., Camuffo, D., Cornes, R., Cram, T. A., Crouthamel, R., . . . Wyszynski, P. (2019). Towards a more reliable historical reanalysis: Improvements for version 3 of the Twentieth Century Reanalysis system. *Quarterly Journal of the Royal Meteorological Society*, *145*(724), 2876-2908. https://doi.org/10.1002/qj.3598

Stevenson, S., Wittenberg, A. T., Fasullo, J., Coats, S., & Otto-Bliesner, B. (2021). Understanding Diverse Model Projections of Future Extreme El Nino. *Journal of Climate*, *34*(2), 449-464. https://doi.org/10.1175/Jcli-D-19-0969.1

Stevenson, S. L. (2012). Significant changes to ENSO strength and impacts in the twenty-first century: Results from CMIP5. *Geophysical Research Letters*, *39*(17). https://doi.org/https://doi.org/10.1029/2012GL052759

Sun, X., Renard, B., Thyer, M., Westra, S., & Lang, M. (2015). A global analysis of the asymmetric effect of ENSO on extreme precipitation. *Journal of Hydrology*, *530*, 51-65. https://doi.org/10.1016/j.jhydrol.2015.09.016

Accepted for publication in *Journal of Climate*. DOI 10.1175/JCLI-D-23-0619.1

Supari, Tangang, F., Salimun, E., Aldrian, E., Sopaheluwakan, A., & Juneng, L. (2018). ENSO modulation of seasonal rainfall and extremes in Indonesia. *Climate Dynamics*, *51*(7-8), 2559-2580. https://doi.org/10.1007/s00382-017-4028-8

Tan, M. L., Juneng, L., Tangang, F. T., Chung, J. X., & Radin Firdaus, R. B. (2021). Changes in temperature extremes and their relationship with ENSO in Malaysia from 1985 to 2018. *International Journal of Climatology*, *41*(S1), E2564-E2580. https://doi.org/https://doi.org/10.1002/joc.6864

Tangang, F., Farzanmanesh, R., Mirzaei, A., Supari, Salimun, E., Jamaluddin, A. F., & Juneng, L. (2017). Characteristics of precipitation extremes in Malaysia associated with El Nino and La Nina events. *International Journal of Climatology*, *37*, 696-716. https://doi.org/10.1002/joc.5032

Taylor, K. E., Stouffer, R. J., & Meehl, G. A. (2012). An Overview of Cmip5 and the Experiment Design. *Bulletin of the American Meteorological Society*, *93*(4), 485-498. https://doi.org/10.1175/Bams-D-11-00094.1

Trenberth, K. E. (1997). The definition of El Nino. *Bulletin of the American Meteorological Society*, *78*(12), 2771-2777. https://doi.org/10.1175/1520-0477(1997)078<2771:Tdoeno>2.0.Co;2

Vicente-Serrano, S. M., López-Moreno, J. I., Gimeno, L., Nieto, R., Morán-Tejeda, E., Lorenzo-Lacruz, J., Beguería, S., & Azorin-Molina, C. (2011). A multiscalar global evaluation of the impact of ENSO on droughts. *Journal of Geophysical Research: Atmospheres*, *116*(D20).

Villafuerte, M. Q., Matsumoto, J., & Kubota, H. (2015). Changes in extreme rainfall in the Philippines (1911-2010) linked to global mean temperature and ENSO. *International Journal of Climatology*, *35*(8), 2033-2044. https://doi.org/10.1002/joc.4105

Ward, P. J., Eisner, S., Florke, M., Dettinger, M. D., & Kummu, M. (2014). Annual flood sensitivities to El Nino-Southern Oscillation at the global scale. *Hydrology and Earth System Sciences*, *18*(1), 47-66. https://doi.org/10.5194/hess-18-47-2014

Westra, S., Alexander, L. V., & Zwiers, F. W. (2013). Global increasing trends in annual maximum daily precipitation. *Journal of Climate*, *26*(11), 3904-3918.

Xiao, M. Z., Zhang, Q., & Singh, V. P. (2015). Influences of ENSO, NAO, IOD and PDO on seasonal precipitation regimes in the Yangtze River basin, China. *International Journal of Climatology*, *35*(12), 3556-3567. https://doi.org/10.1002/joc.4228

Yeh, S. W., Cai, W. J., Min, S. K., McPhaden, M. J., Dommenget, D., Dewitte, B., Collins, M., Ashok, K., An, S. I., Yim, B. Y., & Kug, J. S. (2018). ENSO Atmospheric

Accepted for publication in *Journal of Climate*. DOI 10.1175/JCLI-D-23-0619.1

Teleconnections and Their Response to Greenhouse Gas Forcing. *Reviews of Geophysics*, *56*(1), 185-206. https://doi.org/10.1002/2017rg000568

Yoon, J. H., Wang, S. Y. S., Gillies, R. R., Kravitz, B., Hipps, L., & Rasch, P. J. (2015). Increasing water cycle extremes in California and in relation to ENSO cycle under global warming. *Nature Communications*, *6*. https://doi.org/ARTN 8657 10.1038/ncomms9657

Zhang, Q., Xiao, M. Z., Singh, V. P., & Chen, Y. D. (2014). Max-stable based evaluation of impacts of climate indices on extreme precipitation processes across the Poyang Lake basin, China. *Global and Planetary Change*, *122*, 271-281. https://doi.org/10.1016/j.gloplacha.2014.09.005

Zhang, X., Alexander, L., Hegerl, G. C., Jones, P., Tank, A. K., Peterson, T. C., Trewin, B., & Zwiers, F. W. (2011). Indices for monitoring changes in extremes based on daily temperature and precipitation data. *Wiley Interdisciplinary Reviews: Climate Change*, *2*(6), 851-870.

Zhang, X. B., Wang, J. F., Zwiers, F. W., & Groisman, P. Y. (2010). The Influence of Large-Scale Climate Variability on Winter Maximum Daily Precipitation over North America. *Journal of Climate*, *23*(11), 2902-2915. https://doi.org/10.1175/2010jcli3249.1

Accepted for publication in *Journal of Climate*. DOI 10.1175/JCLI-D-23-0619.1